Strontium ferrite under pressure: Potential analog to strontium ruthenate

Azin Kazemi-Moridani [1,2,*] Sophie Beck [2] Alexander Hampel [2] A.-M. S. Tremblay [3,†]
Michel Côté [1,‡] and Olivier Gingras [2,§]

[1]*Département de Physique, Université de Montréal, 1375 Avenue Thérèse-Lavoie-Roux, Montréal, Québec, Canada H2V 0B3*
[2]*Center for Computational Quantum Physics, Flatiron Institute, 162 Fifth Avenue, New York, New York 10010, USA*
[3]*Département de Physique, Institut quantique, Université de Sherbrooke, Sherbrooke, Québec, Canada J1K 2R1*

As an alternative platform to unravel some of the perplexing characteristics of strontium ruthenate, we propose to study the isostructural and more correlated material strontium ferrite. Using density functional theory combined with dynamical mean-field theory, we attribute the experimentally observed insulating behavior at zero pressure to strong local electronic correlations generated by Mott and Hund's physics. At high pressure, our simulations reproduce the reported insulator-to-metal transition around 18 GPa. Along with distinctive features of a Hund metal, the resulting metallic state is found to display an electronic structure analogous to that of strontium ruthenate, suggesting that it could exhibit similar low-energy properties.

I. INTRODUCTION

The unconventional superconductivity of strontium ruthenate (Sr_2RuO_4, SRO) still fuels debates almost 30 years after its discovery [1–3]. It was the first layered perovskite superconductor to be discovered after the cuprates. However, contrarily to the cuprates, SRO does not necessitate doping to exhibit superconductivity, which allows for investigations in high-quality single crystals. This distinction has motivated extensive studies aimed at characterizing both its normal and superconducting states.

Theoretically, the normal state is nowadays understood as a correlated Hund metal [4,5] with important spin-orbit coupling. Only the t_{2g} electrons of the ruthenium atom play a fundamental role and interactions can be considered local, modeled by the Kanamori Hamiltonian [6–8]. Indeed, the combination of density functional theory (DFT) and dynamical mean-field theory (DMFT) has yielded impressive agreement with experiments, reproducing for example the Fermi surface [9] and the magnetic susceptibility [10]. Additionally, it captures the expected hallmarks of Hund metals such as orbital-selective mass renormalizations [11,12] and a crossover from a bad metal to a Fermi liquid [13,14]. The superconducting state, however, remains enigmatic. The debates persist because thermodynamic measurements supported by theory suggest a one-component order parameter [15–20], while other experiments observed evidence of a two-component order parameter [21–23]. New knobs to turn could help unravel key additional information regarding SRO.

One such knob is simply to study a different, yet similar material. In this regard, our focus turns to strontium ferrite (Sr_2FeO_4, SFO) for which the ruthenium atom (Ru) is replaced with an isoelectronic iron atom (Fe). This substitution results in an increased on-site Coulomb repulsion due to the more localized nature of Fe's $3d$ shell compared to Ru's $4d$ shell, along with a decreased spin-orbit coupling due to the smaller nuclear charge of Fe compared with that of Ru. Our study of SFO is driven by a dual purpose: first, to investigate the distinctive behaviors and electronic properties exhibited by a material with an identical crystal structure to SRO, and second, to harness SFO as a potential source of deeper insights into the elusive physics of SRO's superconducting state. This strategy has been previously successful to shed light on Hund's physics and the role of van Hove singularities by comparing SRO to Sr_2MoO_4 [8].

Because of the unstable tendencies of SFO [24], only a few experiments have been performed on it and in particular no electronic structure calculation has been reported to our knowledge. Experiments on polycrystals report that SFO is an antiferromagnetic insulator with a Néel temperature around 60 K [25–27] and adopts an elliptical cycloidal spin structure below this temperature [28]. Also, a room-temperature insulator-to-metal transition has been detected around 18 GPa [29,30]. Thus, applying pressure to SFO could be a way to suppress the antiferromagnetic order for the benefit of superconductivity, as is observed in many unconventional superconductors [31–34].

In this paper, we explore the correlated electronic structure of unstrained and strained SFO in its normal state above the Néel temperature and compare it to experiments. Starting with DFT, we find that the electronic structure of SFO differs from that of SRO. Indeed, DFT predicts that for SFO, both the e_g and the t_{2g} orbitals cross the Fermi energy and are partially occupied, whereas for SRO, the e_g states are empty while the t_{2g} orbitals are partially occupied. Since SFO is observed to be

*mohaddeseh.kazemi.moridani@umontreal.ca
†andre-marie.tremblay@usherbrooke.ca
‡michel.cote@umontreal.ca
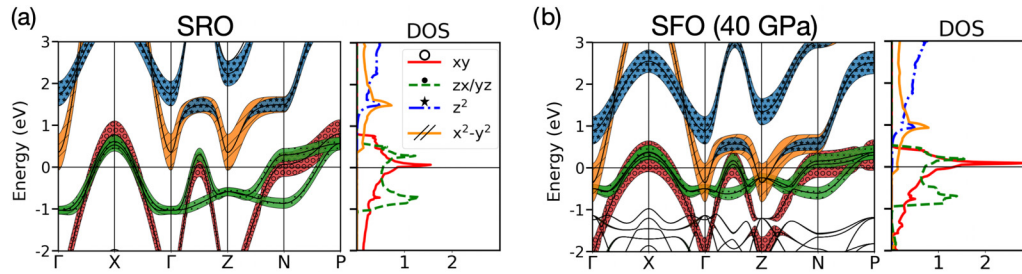§ogingras@flatironinstitute.org

FIG. 1. Comparison of the open d-shell orbital character on the band structure of (a) SRO, and (b) SFO under 40 GPa of isotropic pressure. The d_{xy}, $d_{yz/zx}$, d_{z^2}, and $d_{x^2-y^2}$ orbital characters are shown in red, green, blue, and orange, respectively. The horizontal line at zero marks the Fermi energy. The e_g orbitals are unoccupied in SRO while the $d_{x^2-y^2}$ orbital is slightly metallic in SFO at 40 GPa.

insulating, we correct this prediction by incorporating dynamical local correlations within DMFT. Although SFO has been categorized as a negative charge-transfer insulator in previous works [28], here we explore the rich phase diagram generated by the Fe atom's on-site Coulomb repulsion U and Hund's coupling J. We argue that for $U \geqslant 2.5$ eV and $J < 0.7$ eV, we obtain the phase most consistent with experiments. This value of U is slightly above the one predicted using the constrained random phase approximation (cRPA). In this phase, the e_g states are pushed above the Fermi energy, while the remaining electrons in the t_{2g} shell become Mott insulating. We show that this phase undergoes an insulator-metal transition around 18 GPa of isotropic pressure, consistent with experiments. By comparing the band structure, the Fermi surface, and the mass enhancements of this metallic phase with that of SRO, we reveal an exciting similarity between the two, suggesting SFO as an alternative platform to understand SRO.

II. DFT ELECTRONIC STRUCTURE

SFO (SRO) crystallizes in a body-centered-tetragonal structure with Fe (Ru) at the center of FeO$_6$ (RuO$_6$) octahedra. The crystal field generated by the p orbitals of the surrounding oxygen atoms splits the fivefold degeneracy of the Fe d shell into an e_g doublet ($d_{x^2-y^2}$ and d_{z^2} orbitals) and a t_{2g} triplet (d_{xy}, d_{zx} and d_{yz} orbitals).

Figure 1 presents the band structures of both SRO [Fig. 1(a)] and SFO [Fig. 1(b)] at 40 GPa obtained using DFT. The details of the calculations can be found in the Supplemental Material (SM) [35]. We show the projection of the wave function onto the d orbitals of the transition metal element, along with the orbital-selective densities of states (DOS). Note that the electronic structure of SFO without pressure is qualitatively similar to the one at 40 GPa [35]. In SRO, the band dispersion reveals an overlap between the e_g and t_{2g} orbitals, but only the t_{2g} orbitals are partially filled and cross the Fermi level while the e_g orbitals remain completely unoccupied. Thus, as was done in most theoretical studies of SRO [6–10,12,14,18–20], one can focus solely on the t_{2g} orbitals.

However, in the case of SFO, both the t_{2g} and $d_{x^2-y^2}$ orbitals are active at the Fermi level, necessitating a minimal model that includes the e_g orbitals to describe the low-energy physics accurately.

In short, although the noninteracting band structure of SFO is similar to SRO's, the presence of e_g electrons at the Fermi

level is a massive distinction. Moreover, we have been neglecting so far the role of strong electronic correlations. In SRO, although important, they do not significantly affect the Fermi surface itself [36]. In contrast, experiments on SFO observe an insulating state rather than a metallic one. We now investigate whether the correlation effects among the Fe d electrons can be responsible for this discrepancy with DFT.

III. STRONG CORRELATIONS

Because of the localized nature of 3d orbitals, SFO is expected to be affected by strong electronic correlations. This is reinforced by the disagreement between the *ab initio* prediction of a metallic state and the experimental observation of an insulating state. We now incorporate the missing local electronic correlations from DFT using DMFT. This is done by projecting the DFT Kohn-Sham wave function onto a downfolded model considering only the five 3d orbitals of the Fe atom and constructed using the WANNIER90 package. The correlations are obtained by iteratively solving the impurity model using DMFT, with the interactions modeled by the full rotationally invariant Slater Hamiltonian (including non-density-density terms) which depends on two parameters: the strength of the electronic Coulomb repulsion U and the Hund's coupling J. Details about the downfolding, the numerical calculations, and the Slater Hamiltonian parametrization can be found in the SM [35].

We explore possible electronic states of SFO by investigating the U-J parameter space of the full Slater Hamiltonian. The phase diagram in Fig. 2 summarizes our findings for a temperature of 146 K ($1/k_B T = 80$ eV^{-1}). Based on observables such as the spectral function [35] and the resulting orbital occupations, we classify the phases using three types of colored markers: the blue triangles, red squares, and green stars, corresponding to the t_{2g} orbitals being metallic, being insulating due to correlations, or being orbital-selectively insulating, respectively. For the first two classes (triangles and squares), a solid (open) symbol represents metallic (band insulating) e_g orbitals, while a half-solid symbol indicates that only the $d_{x^2-y^2}$ orbital is metallic. For the third class (stars), the d_{xy} and e_g orbitals are found metallic, while the $d_{zx/yz}$ ones are Mott insulating. We call this phase the orbital-selective Mott phase (OSMP).

We now discuss the different phases and physical mechanisms leading to the phase diagram shown in Fig. 2. Additional information can be found in the SM [35]. In the
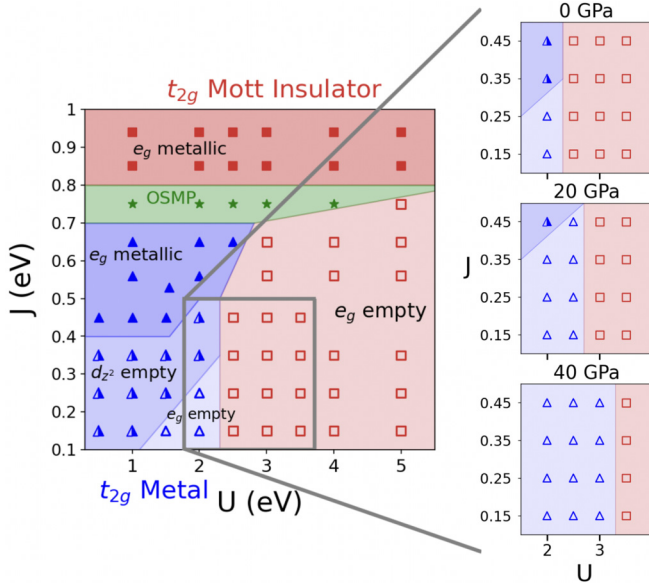
FIG. 2. Phase diagrams of SFO in the space of the interaction parameters at $T = 146$ K for three pressures. Here, the Hund's coupling J and on-site Coulomb repulsion U are expressed in the Slater definition. The red squares distinguish Mott insulating t_{2g} orbitals, whereas the blue triangles correspond to metallic t_{2g} orbitals. The filling of the markers reflects whether both e_g orbitals are partially occupied (solid), only the $d_{x^2-y^2}$ is partially occupied (half solid), or none are (open). The narrow region with green stars corresponds to an orbital-selective Mott phase (OSMP) with d_{xy} and e_g metallic, and $d_{zx/yz}$ Mott insulating. On the right, a selected region is compared for three different pressures: 0, 20, and 40 GPa. It highlights the insulator-to-metal transition observed around 18 GPa [29,30] for $U \sim 2.5$ eV, where the resulting metallic states have empty e_g orbitals.

low U and low J regime depicted by half-solid blue triangles, we find the DFT solution shown in Fig. 1(b) where only the d_{z^2} orbital is empty. As mentioned before, experimental observations suggest SFO to be a small gap insulator at zero pressure [25–27]. We find the phase that best reproduces these observations at larger U: the phase marked by open red squares where all orbitals are insulating. This phase emerges by increasing the cost of double occupancy U because it suppresses charge fluctuations and constrains the Fe atoms to host four localized electrons. Due to the crystal field splitting generated by the oxygen atoms surrounding the Fe atom, the d_{xy} orbital has the lowest on-site energy and is getting fully filled, the e_g orbitals have the highest on-site energies and are pushed above the Fermi level making them band insulating, and the $d_{yz/zx}$ orbitals have to share two electrons which makes them Mott insulating.

This phase, most consistent with experimental observations at zero pressure, is found roughly in the parameter regime $U \geqslant 2.5$ eV and $J < 0.7$ eV. Using the cRPA to calculate the screened interaction parameters [35], we find the static values (zero frequency limit) to be U_{cRPA}, $J_{cRPA} =$ 1.5 eV, 0.5 eV. Although these numbers are outside of the region deemed realistic, it is known that cRPA overestimates screening effects, leading to underestimated U values [37,38]. Considering this fact, U_{cRPA} appears reasonably close to the

empty red square region. Now, to attain a deeper understanding of the physical mechanisms at play and guide possible fine tuning, we continue analyzing the full phase diagram.

If again we start from the small U and small J region, but this time go along the direction of increasing J instead of U, we see that the occupancies of the e_g orbitals start to increase. This happens because of the Hund's rule, which states that J favors spin alignment and thus spreads the orbital occupation throughout the entire d shell, making all orbitals metallic at some point. Eventually at very large J, there is enough occupation transfer from the t_{2g} to the e_g orbitals so that a Mott gap opens up in t_{2g} while e_g remains metallic: First, the Mott gap opens in the less occupied $d_{yz/zx}$ orbital (leading to the green star phase), and then in the d_{xy} orbital, resulting in the t_{2g} insulating and e_g metallic phase (solid red square phase).

Finally, another remarkable result from the phase diagram of Fig. 2 is the empty blue triangle phase, which has band-insulating e_g and partially filled t_{2g} orbitals. This configuration is analogous to that of SRO and could offer an alternative route to study the physics of this important system. Since this metallic phase is on the border with the realistic insulating phase, we believe isotropic pressure might actually allow us to realize this metallic phase.

IV. INSULATOR-TO-METAL TRANSITION

In this section, we explore the insulator-to-metal transition of SFO under pressure and show that the metallic phase can be fine tuned to have a similar band structure and Fermi surface to that of SRO. The insulator-to-metal transition observed experimentally happens around 18 GPa at room temperature [29,30]. Our results naturally predict that this critical pressure should be temperature dependent, which can be tested experimentally. To investigate this insulator-to-metal transition, we restricted our simulation to a window near the phase transition between the insulating (the empty red square phase) and the metallic phases. The right panels of Fig. 2 present this evolution for three pressures: 0, 20, and 40 GPa. We preserve the original crystalline symmetry, in agreement with experiments that confirmed this up to 30 GPa [29,30,39].

Increasing pressure increases the propensity of electrons to hop from site to site t, i.e., it increases the bandwidth of the d shell without significantly affecting the Coulomb repulsion U. Consequently, the effective Coulomb repulsion U/t decreases. This effect results in the expansion of the metallic state within the parameter space as shown on the right of Fig. 2, while also providing a clear explanation for the insulator-to-metal transition observed in experiments. Moreover, this effect suggests that the boundary between the metallic and insulating regions should move with temperature, leading to a temperature-dependent critical pressure for the insulator-to-metal transition. Experiments could already be performed to test this prediction.

We now focus on the region where both e_g orbitals are empty, which we observe also grows with pressure. This is likely due to the modified competition between the crystal field and Hund's coupling J. Indeed, applying pressure on the material increases the crystal field splitting which favors low-spin states and pushes the e_g orbitals further away in
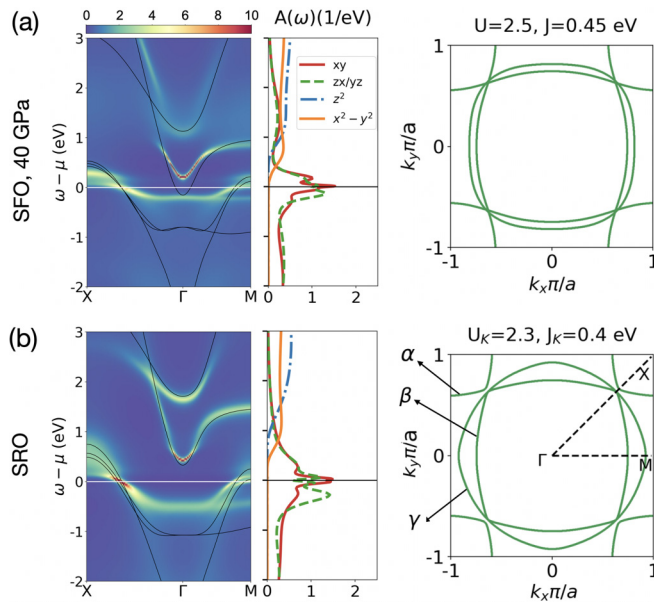
FIG. 3. Correlated band structure on the left, DOS in the middle, and Fermi surface on the right of (a) 40 GPa SFO in the three-orbital metallic phase and (b) SRO, both at $T = 146$ K. The DFT result is represented by the black lines. Clearly, correlations push e_g orbitals away from the Fermi level. The Fermi surfaces are labeled α, β, γ in (b). The parameters for the calculations are on top of the Fermi surfaces. Although calculations for both of the materials rely on the Slater Hamiltonian, SRO's parameters are presented in the Kanamori convention to ease the comparison with previous studies. The corresponding values of SRO in Slater are $U = 1.66$ eV and $J = 0.56$ eV. See Eqs. (S30) and (S31) of the SM for conversion relations between Slater and Kanamori values.

energy. In contrast, J favors a high-spin state and spreads the orbital occupations. Thus, with increasing pressure, a larger J is required to occupy the e_g orbitals. Therefore the empty blue triangle region that represents a metallic phase with empty e_g orbitals expands.

In order to compare the three-orbital metallic phase of SFO found under pressure with SRO, we present their respective correlated band structures, DOS, and Fermi surfaces in Fig. 3. What is meant by these *correlated* objects is detailed in the SM [35]. In Fig. 3(a), we display the 40 GPa phase of SFO to highlight a case at higher pressure, and we selected $U = 2.5$ eV and $J = 0.45$ eV as an example that reproduces the experimental observations with physically relevant parameters. In the first panel, we contrast the correlated band structure with the one obtained using DFT and one clearly sees that correlations have pushed the e_g orbitals away from the Fermi level compared to Fig. 1(b).

Comparing the corresponding quantities for both systems, we argue that SFO in this particular phase is analogous to SRO. Both are metals with four t_{2g} electrons, three similar Fermi sheets, and comparable DOSs with a van Hove singularity in the vicinity of the Fermi energy. There are, however, two important differences between the two, which can be regarded as opportunities: First, even with pressure, the bandwidth of SFO remains smaller, implying stronger electronic correlations than in SRO. Since higher pressure should

bring it to a value similar to that of SRO, this represents an opportunity to study continuously a more correlated version of SRO. This increased strength of interaction should lead to stronger magnetic fluctuations which can promote a magnetic order, or possibly superconductivity.

Second, the γ sheet of the Fermi surface of SFO is more squarelike than that of SRO. While the calculations presented here do not include spin-orbit coupling, it should not have an important impact on SFO because of the small charge of Fe's nuclei. As a result, the squareness of the γ sheet presented for SFO in Fig. 3(a) should remain similar, leading to a larger nesting than in SRO. Nesting itself leads to an increased strength of the spin fluctuations. More studies need to be performed on these speculations.

In addition to the observables presented above, we demonstrate that the three-orbital metallic phase that we find for SFO displays distinctive features of Hund metals [4,5,12]. This is highlighted by inspecting the effect of Hund's coupling J on the orbital-selective effective mass enhancements $\frac{m^*}{m_{\text{DFT}}}|_l$ and on the scattering rates Γ_l. These quantities measure the degree of electronic correlations missing from DFT and captured by DMFT. They are reported in the SM [35]. Indeed, three points stand out: First, we find that the mass enhancements and the scattering rates all increase with J. Second, the effective mass of the xy orbital increases faster than those of the yz/zx orbitals. Third, the larger J, the lower we have to go in temperature before the effective masses saturate. This last point highlights that it is increasingly challenging to reach the coherent regime where quasiparticles are well defined, that is, the Fermi-liquid regime. The considerable increase in correlation, orbital differentiation due to J and pushing of the Fermi-liquid scale to lower temperatures due to J are all hallmarks of Hund metals [4,5]. They are also observed in SRO [12], thus supporting further the analogy between SFO and SRO. We note that reaching the coherent regime at large J is especially challenging for five-orbital systems, thus we plan on extracting the effective masses that would be measured experimentally in future works.

V. CONCLUSION

We studied the correlated electronic structure of strontium ferrite, Sr_2FeO_4, using a combination of density functional theory and dynamical mean-field theory. Correctly capturing correlation effects of the Fe d electrons is essential to reproduce the experimentally observed insulating state of Sr_2FeO_4. We find such a state for interaction strengths $U > 2.5$ eV, where only the t_{2g} orbitals are occupied. Moreover, we are able to reproduce the experimentally observed insulator-to-metal transition in Sr_2FeO_4 under pressure. The metallic state of Sr_2FeO_4 at 40 GPa with $U > 2.5$ eV displays the distinctive features of Hund metals and offers a promising analog state to Sr_2RuO_4, for which correlations could be tuned with additional pressure. Indeed, both of these states are metals with four electrons in their t_{2g} shells with similar band structures, density of states, and Fermi surfaces. The difference is that the effective mass enhancement is generally larger in SFO, and the nesting of its Fermi surface is suggestive of enhanced magnetic fluctuations that may lead to superconductivity.

[1] Y. Maeno, H. Hashimoto, K. Yoshida, S. Nishizaki, T. Fujita, J. G. Bednorz, and F. Lichtenberg, Superconductivity in a layered perovskite without copper, Nature (London) **372**, 532 (1994).

[2] A. P. Mackenzie, R. K. W. Haselwimmer, A. W. Tyler, G. G. Lonzarich, Y. Mori, S. Nishizaki, and Y. Maeno, Extremely strong dependence of superconductivity on disorder in Sr_2RuO_4, Phys. Rev. Lett. **80**, 161 (1998).

[3] A. P. Mackenzie, T. Scaffidi, C. W. Hicks, and Y. Maeno, Even odder after twenty-three years: The superconducting order parameter puzzle of Sr_2RuO_4, npj Quantum Mater. **2**, 40 (2017).

[4] A. Georges, L de' Medici, and J. Mravlje, Strong correlations from Hund's coupling, Annu. Rev. Condens. Matter Phys. **4**, 137 (2013).

[5] L. de' Medici, J. Mravlje, and A. Georges, Janus-faced influence of Hund's rule coupling in strongly correlated materials, Phys. Rev. Lett. **107**, 256401 (2011).

[6] T. Mizokawa and A. Fujimori, Unrestricted Hartree-Fock study of transition-metal oxides: Spin and orbital ordering in perovskite-type lattice, Phys. Rev. B **51**, 12880(R) (1995).

[7] M. Zingl, J. Mravlje, M. Aichhorn, O. Parcollet, and A. Georges, Hall coefficient signals orbital differentiation in the Hund's metal Sr_2RuO_4, npj Quantum Mater. **4**, 35 (2019).

[8] J. Karp, M. Bramberger, M. Grundner, U. Schollwöck, A. J. Millis, and M. Zingl, Sr_2MoO_4 and Sr_2RuO_4: Disentangling the roles of Hund's and van Hove physics, Phys. Rev. Lett. **125**, 166401 (2020).

[9] A. Tamai, M. Zingl, E. Rozbicki, E. Cappelli, S. Ricco, A. de la Torre, S. McKeown Walker, F. Y. Bruno, P. D. C. King, W. Meevasana, M. Shi, M. Radovic, N. C. Plumb, A. S. Gibbs, A. P. Mackenzie, C. Berthod, H. U. R. Strand, M. Kim, A. Georges, and F. Baumberger, High-resolution photoemission on Sr_2RuO_4 reveals correlation-enhanced effective spin-orbit coupling and dominantly local self-energies, Phys. Rev. X **9**, 021048 (2019).

[10] H. U. R. Strand, M. Zingl, N. Wentzell, O. Parcollet, and A. Georges, Magnetic response of Sr_2RuO_4: Quasi-local spin fluctuations due to Hund's coupling, Phys. Rev. B **100**, 125120 (2019).

[11] C. Bergemann, J. S. Brooks, L. Balicas, A. P. Mackenzie, S. R. Julian, Z. Q. Mao, and Y. Maeno, Normal state of the unconventional superconductor Sr_2RuO_4 in high magnetic fields, Physica B: Condens. Matter **294-295**, 371 (2001).

[12] J. Mravlje, M. Aichhorn, T. Miyake, K. Haule, G. Kotliar, and A. Georges, Coherence-incoherence crossover and the mass-renormalization puzzles in Sr_2RuO_4, Phys. Rev. Lett. **106**, 096401 (2011).

[13] N. E. Hussey, A. P. Mackenzie, J. R. Cooper, Y. Maeno, S. Nishizaki, and T. Fujita, Normal-state magnetoresistance of Sr_2RuO_4, Phys. Rev. B **57**, 5505 (1998).

[14] F. B. Kugler, M. Zingl, H. U. R. Strand, S.-S. B. Lee, J. von Delft, and A. Georges, Strongly correlated materials from a numerical renormalization group perspective: How the Fermi-liquid state of Sr_2RuO_4 emerges, Phys. Rev. Lett. **124**, 016401 (2020).

[15] E. Hassinger, P. Bourgeois-Hope, H. Taniguchi, S. René de Cotret, G. Grissonnanche, M. S. Anwar, Y. Maeno, N. Doiron-Leyraud, and L. Taillefer, Vertical line nodes in the superconducting gap structure of Sr_2RuO_4, Phys. Rev. X **7**, 011032 (2017).

[16] Y.-S. Li, M. Garst, J. Schmalian, S. Ghosh, N. Kikugawa, D. A. Sokolov, C. W. Hicks, F. Jerzembeck, M. S. Ikeda, Z. Hu, B. J. Ramshaw, A. W. Rost, M. Nicklas, and A. P. Mackenzie, Elastocaloric determination of the phase diagram of Sr_2RuO_4, Nature (London) **607**, 276 (2022).

[17] Y.-S. Li, N. Kikugawa, D. A. Sokolov, F. Jerzembeck, A. S. Gibbs, Y. Maeno, C. W. Hicks, J. Schmalian, M. Nicklas, and A. P. Mackenzie, High-sensitivity heat-capacity measurements on Sr_2RuO_4 under uniaxial pressure, Proc. Natl. Acad. Sci. USA **118**, e2020492118 (2021).

[18] O. Gingras, R. Nourafkan, A.-M. S. Tremblay, and M. Côté, Superconducting symmetries of Sr_2RuO_4 from first-principles electronic structure, Phys. Rev. Lett. **123**, 217005 (2019).

[19] O. Gingras, N. Allaglo, R. Nourafkan, M. Côté, and A.-M. S. Tremblay, Superconductivity in correlated multiorbital systems with spin-orbit coupling: Coexistence of even- and odd-frequency pairing, and the case of Sr_2RuO_4, Phys. Rev. B **106**, 064513 (2022).

[20] J. B. Profe, S. Beck, D. M. Kennes, A. Georges, and O. Gingras, Competition between d-wave superconductivity and magnetism in uniaxially strained Sr_2RuO_4, arXiv:2307.10006.

[21] S. Benhabib, C. Lupien, I. Paul, L. Berges, M. Dion, M. Nardone, A. Zitouni, Z. Q. Mao, Y. Maeno, A. Georges, L. Taillefer, and C. Proust, Ultrasound evidence for a two-component superconducting order parameter in Sr_2RuO_4, Nat. Phys. **17**, 194 (2021).

[22] S. Ghosh, A. Shekhter, F. Jerzembeck, N. Kikugawa, D. A. Sokolov, M. Brando, A. P. Mackenzie, C. W. Hicks, and B. J. Ramshaw, Thermodynamic evidence for a two-component superconducting order parameter in Sr_2RuO_4, Nat. Phys. **17**, 199 (2021).

[23] V. Grinenko, S. Ghosh, R. Sarkar, J.-C. Orain, A. Nikitin, M. Elender, D. Das, Z. Guguchia, F. Brückner, M. E. Barber, J. Park, N. Kikugawa, D. A. Sokolov, J. S. Bobowski, T. Miyoshi,

Y. Maeno, A. P. Mackenzie, H. Luetkens, C. W. Hicks, and H.-H. Klauss, Split superconducting and time-reversal symmetry-breaking transitions in Sr_2RuO_4 under stress, Nat. Phys. **17**, 748 (2021).

[24] A. Fossdal, M.-A. Einarsrud, and T. Grande, Phase equilibria in the pseudo-binary system $SrO-Fe_2O_3$, J. Solid State Chem. **177**, 2933 (2004).

[25] S. E. Dann, M. T. Weller, and D. B. Currie, The synthesis and structure of Sr_2FeO_4, J. Solid State Chem. **92**, 237 (1991).

[26] S. E. Dann, M. T. Weller, D. B. Currie, M. F. Thomas, and A. D. Al-Rawwas, Structure and magnetic properties of Sr_2FeO_4 and $Sr_3Fe_2O_7$ studied by powder neutron diffraction and Mössbauer spectroscopy, J. Mater. Chem. **3**, 1231 (1993).

[27] P. Adler, Properties of K_2NiF_4-type oxides Sr_2FeO_4, J. Solid State Chem. **108**, 275 (1994).

[28] P. Adler, M. Reehuis, N. Stüßer, S. A. Medvedev, M. Nicklas, D. C. Peets, J. Bertinshaw, C. K. Christensen, M. Etter, A. Hoser, L. Schröder, P. Merz, W. Schnelle, A. Schulz, Q. Mu, D. Bessas, A. Chumakov, M. Jansen, and C. Felser, Spiral magnetism, spin flop, and pressure-induced ferromagnetism in the negative charge-transfer-gap insulator Sr_2FeO_4, Phys. Rev. B **105**, 054417 (2022).

[29] G. R. Hearne, M. P. Pasternak, and R. D. Taylor, Selected studies of magnetism at high pressure, Nuovo Cim. **18**, 145 (1996).

[30] G. K. Rozenberg, A. P. Milner, M. P. Pasternak, G. R. Hearne, and R. D. Taylor, Experimental confirmation of a p-p intraband gap in Sr_2FeO_4, Phys. Rev. B **58**, 10283 (1998).

[31] R. Brusetti, M. Ribault, D. Jérome, and K. Bechgaard, Insulating, conducting and superconducting states of $(TMTSF)_2AsF_6$ under pressure and magnetic field, J. Phys. France **43**, 801 (1982).

[32] N. D. Mathur, F. M. Grosche, S. R. Julian, I. R. Walker, D. M. Freye, R. K. W. Haselwimmer, and G. G. Lonzarich, Magnetically mediated superconductivity in heavy fermion compounds, Nature (London) **394**, 39 (1998).

[33] S. Lefebvre, P. Wzietek, S. Brown, C. Bourbonnais, D. Jérome, C. Mézière, M. Fourmigué, and P. Batail, Mott transition, antiferromagnetism, and unconventional superconductivity in layered organic superconductors, Phys. Rev. Lett. **85**, 5420 (2000).

[34] N. Doiron-Leyraud, P. Auban-Senzier, S. René de Cotret, C. Bourbonnais, D. Jérome, K. Bechgaard, and L. Taillefer, Correlation between linear resistivity and T_c in the Bechgaard salts and the pnictide superconductor $Ba(Fe_{1-x}Co_x)_2As_2$, Phys. Rev. B **80**, 214531 (2009).

[35] See Supplemental Material at http://link.aps.org/supplemental/10.1103/PhysRevB.109.165146 for the computational details, the classification and mechanisms found in the phase diagram, strained and unstrained band structures of Sr_2FeO_4 obtained from DFT, the connection between Slater and Kanamori Hamiltonians, the definitions of correlated band structure and the quasiparticle Fermi surface, in addition to the mass enhancement of Sr_2FeO_4, which includes Refs. [37,38,40–70].

[36] G. Zhang, E. Gorelov, E. Sarvestani, and E. Pavarini, Fermi surface of Sr_2RuO_4: Spin-orbit and anisotropic Coulomb interaction effects, Phys. Rev. Lett. **116**, 106402 (2016).

[37] M. Casula, P. Werner, L. Vaugier, F. Aryasetiawan, T. Miyake, A. J. Millis, and S. Biermann, Low-energy models for correlated materials: Bandwidth renormalization from Coulombic screening, Phys. Rev. Lett. **109**, 126408 (2012).

[38] C. Honerkamp, H. Shinaoka, F. F. Assaad, and P. Werner, Limitations of constrained random phase approximation downfolding, Phys. Rev. B **98**, 235151 (2018).

[39] P. Adler, A. F. Goncharov, K. Syassen, and E. Schönherr, Optical reflectivity and Raman spectra of Sr_2FeO_4 under pressure, Phys. Rev. B **50**, 11396 (1994).

[40] P. Hohenberg and W. Kohn, Inhomogeneous electron gas, Phys. Rev. **136**, B864 (1964).

[41] W. Kohn and L. J. Sham, Self-consistent equations including exchange and correlation effects, Phys. Rev. **140**, A1133 (1965).

[42] W. Kohn, A. D. Becke, and R. G. Parr, Density functional theory of electronic structure, J. Phys. Chem. **100**, 12974 (1996).

[43] G. Pizzi, V. Vitale, R. Arita, S. Blügel, F. Freimuth, G. Géranton, M. Gibertini, D. Gresch, C. Johnson, T. Koretsune, J. Ibañez-Azpiroz, H. Lee, J.-M. Lihm, D. Marchand, A. Marrazzo, Y. Mokrousov, J. I. Mustafa, Y. Nohara, Y. Nomura, L. Paulatto *et al.*, Wannier90 as a community code: new features and applications, J. Phys.: Condens. Matter **32**, 165902 (2020).

[44] A. Georges, G. Kotliar, W. Krauth, and M. J. Rozenberg, Dynamical mean-field theory of strongly correlated fermion systems and the limit of infinite dimensions, Rev. Mod. Phys. **68**, 13 (1996).

[45] K. Held, Electronic structure calculations using dynamical mean field theory, Adv. Phys. **56**, 829 (2007).

[46] G. Kotliar, S. Y. Savrasov, K. Haule, V. S. Oudovenko, O. Parcollet, and C. A. Marianetti, Electronic structure calculations with dynamical mean-field theory, Rev. Mod. Phys. **78**, 865 (2006).

[47] X. Gonze, B. Amadon, G. Antonius, F. Arnardi, L. Baguet, J.-M. Beuken, J. Bieder, F. Bottin, J. Bouchet, E. Bousquet, N. Brouwer, F. Bruneval, G. Brunin, T. Cavignac, J.-B. Charraud, W. Chen, M. Côté, S. Cottenier, J. Denier, G. Geneste *et al.*, The ABINIT project: Impact, environment and recent developments, Comput. Phys. Commun. **248**, 107042 (2020).

[48] A. H. Romero, D. C. Allan, B. Amadon, G. Antonius, T. Applencourt, L. Baguet, J. Bieder, F. Bottin, J. Bouchet, E. Bousquet, F. Bruneval, G. Brunin, D. Caliste, M. Côté, J. Denier, C. Dreyer, P. Ghosez, M. Giantomassi, Y. Gillet, O. Gingras *et al.*, ABINIT: Overview and focus on selected capabilities, J. Chem. Phys. **152**, 124102 (2020).

[49] P. E. Blöchl, Projector augmented-wave method, Phys. Rev. B **50**, 17953 (1994).

[50] M. Torrent, F. Jollet, F. Bottin, G. Zérah, and X. Gonze, Implementation of the projector augmented-wave method in the ABINIT code: Application to the study of iron under pressure, Comput. Mater. Sci. **42**, 337 (2008).

[51] F. Jollet, M. Torrent, and N. Holzwarth, Generation of projector augmented-wave atomic data: A 71 element validated table in the XML format, Comput. Phys. Commun. **185**, 1246 (2014).

[52] M. J. van Setten, M. Giantomassi, E. Bousquet, M. J. Verstraete, D. R. Hamann, X. Gonze, and G.-M. Rignanese, The PseudoDojo: Training and grading a 85 element optimized norm-conserving pseudopotential table, Comput. Phys. Commun. **226**, 39 (2018).

[53] A. Jain, S. P. Ong, G. Hautier, W. Chen, W. D. Richards, S. Dacek, S. Cholia, D. Gunter, D. Skinner, G. Ceder, and K. A. Persson, Commentary: The Materials Project: A materials

genome approach to accelerating materials innovation, APL Mater. **1**, 011002 (2013).

[54] O. Parcollet, M. Ferrero, T. Ayral, H. Hafermann, I. Krivenko, L. Messio, and P. Seth, TRIQS: A toolbox for research on interacting quantum systems, Comput. Phys. Commun. **196**, 398 (2015).

[55] J. Kanamori, Electron correlation and ferromagnetism of transition metals, Prog. Theor. Phys. **30**, 275 (1963).

[56] M. Aichhorn, L. Pourovskii, P. Seth, V. Vildosola, M. Zingl, O. E. Peil, X. Deng, J. Mravlje, G. J. Kraberger, C. Martins, M. Ferrero, and O. Parcollet, TRIQS/DFTTools: A TRIQS application for *ab initio* calculations of correlated materials, Comput. Phys. Commun. **204**, 200 (2016).

[57] P. Werner, A. Comanac, L. de' Medici, M. Troyer, and A. J. Millis, Continuous-time solver for quantum impurity models, Phys. Rev. Lett. **97**, 076405 (2006).

[58] E. Gull, P. Werner, S. Fuchs, B. Surer, T. Pruschke, and M. Troyer, Continuous-time quantum Monte Carlo impurity solvers, Comput. Phys. Commun. **182**, 1078 (2011).

[59] P. Seth, I. Krivenko, M. Ferrero, and O. Parcollet, TRIQS/CTHYB: A continuous-time quantum Monte Carlo hybridisation expansion solver for quantum impurity problems, Comput. Phys. Commun. **200**, 274 (2016).

[60] L. Boehnke, H. Hafermann, M. Ferrero, F. Lechermann, and O. Parcollet, Orthogonal polynomial representation of imaginary-time Green's functions, Phys. Rev. B **84**, 075145 (2011).

[61] M. E. Merkel, A. Carta, S. Beck, and A. Hampel, solid_dmft: Gray-boxing DFT+DMFT materials simulations with TRIQS, J. Open Source Softw. **7**, 4623 (2022).

[62] G. J. Kraberger, R. Triebl, M. Zingl, and M. Aichhorn, Maximum entropy formalism for the analytic continuation of matrix-valued Green's functions, Phys. Rev. B **96**, 155128 (2017).

[63] R. N. Silver, D. S. Sivia, and J. E. Gubernatis, Maximum-entropy method for analytic continuation of quantum Monte Carlo data, Phys. Rev. B **41**, 2380 (1990).

[64] J. E. Gubernatis, M. Jarrell, R. N. Silver, and D. S. Sivia, Quantum Monte Carlo simulations and maximum entropy: Dynamics from imaginary-time data, Phys. Rev. B **44**, 6011 (1991).

[65] M. Jarrell and J. E. Gubernatis, Bayesian inference and the analytic continuation of imaginary-time quantum Monte Carlo data, Phys. Rep. **269**, 133 (1996).

[66] F. Aryasetiawan, M. Imada, A. Georges, G. Kotliar, S. Biermann, and A. I. Lichtenstein, Frequency-dependent local interactions and low-energy effective models from electronic structure calculations, Phys. Rev. B **70**, 195104 (2004).

[67] K. Nakamura, Y. Yoshimoto, Y. Nomura, T. Tadano, M. Kawamura, T. Kosugi, K. Yoshimi, T. Misawa, and Y. Motoyama, RESPACK: An *ab initio* tool for derivation of effective low-energy model of material, Comput. Phys. Commun. **261**, 107781 (2021).

[68] L. Vaugier, H. Jiang, and S. Biermann, Hubbard *U* and Hund exchange *J* in transition metal oxides: Screening versus localization trends from constrained random phase approximation, Phys. Rev. B **86**, 165105 (2012).

[69] P. Seth, P. Hansmann, A. van Roekeghem, L. Vaugier, and S. Biermann, Towards a first-principles determination of effective Coulomb interactions in correlated electron materials: Role of intershell interactions, Phys. Rev. Lett. **119**, 056401 (2017).

[70] E. Şaşıoğlu, C. Friedrich, and S. Blügel, Effective Coulomb interaction in transition metals from constrained random-phase approximation, Phys. Rev. B **83**, 121101(R) (2011).